

Supplemental Material

Electronic Structure of Au₂₅ Clusters: Between Discrete and Continuous

Khabiboulakh Katsiev[†], Nataliya Lozova[‡], Lu Wang^{††}, Katla Sai Krishna[‡], Ruipeng Li^{‡‡}, Wai-Ning Mei^{††}, Sara E. Skrabalak[§], Challa S. S. R. Kumar^{‡}, and Yaroslav Losovyj^{*§}*

[†]Department of Chemistry, University of Texas at Austin, Austin, Texas 78712, United States

[§]Department of Chemistry, Indiana University, Bloomington, Indiana 47405, United States

^{††}Department of Physics, University of Nebraska at Omaha, Omaha, Nebraska 68182, United States

[‡]Center for Atomic-Level Catalyst Design, Cain Department of Chemical Engineering, Center for Advanced Microstructures and Devices (CAMD), Louisiana State University, Baton Rouge, Louisiana 70806, United States

^{‡‡}Cornell High Energy Synchrotron Source (CHESS), Cornell University, Ithaca, New York 14850, United States

*Corresponding Authors

ylozovyj@indiana.edu:

ckumar@lsu.edu

A schematic representation of transition from quantized states to hybridized band in $[\text{Au}_{25}(\text{PPh}_3)_{10}(\text{SC}_{12}\text{H}_{25})_5\text{Cl}_2]^{2+} - (\text{Au}_{25}\text{-bi})$

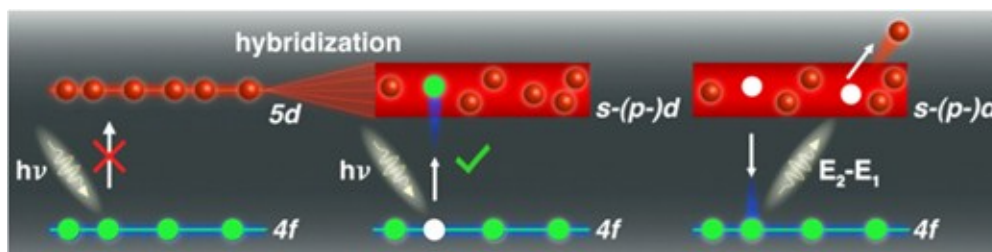


Figure S1. Illustration of resonant photoemission process in gold. An isolated gold atom or molecule is a filled $5d^{10}6s^1$ system, thus electron transition from $4f$ to $5d$ atomic orbital is forbidden. Such an electron transition is only permitted in the presence of the s-d hybridization of the orbitals, leading to a partial depletion of the d-band. This allows for the photoemission transition to a (s - d hybridized) $5d$ states at the $4f_{7/2}$ and $4f_{5/2}$ threshold, resulting in the resonant photoemission enhancement.

UV-Visible spectra of the Au_{25} clusters:

Optical absorbances of the samples were recorded using Shimadzu, UV-3600 spectrophotometer. 3 ml of sample (in dichloromethane or toluene) was introduced into 10 mm-wide Quartz cuvette and the absorbance was measured from 250 nm to 900 nm. The absorbance bands for respective samples were assigned based on previously published reports.

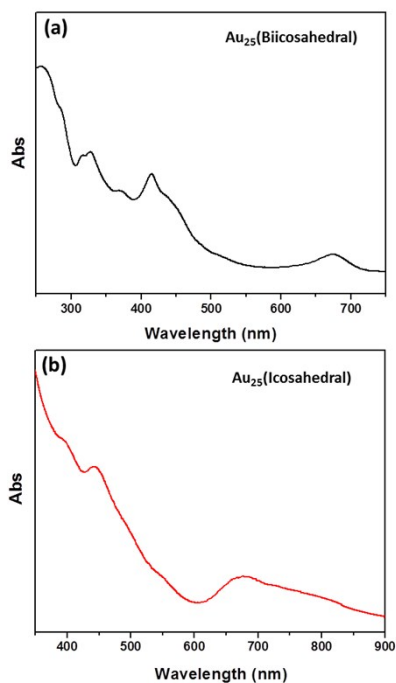


Figure S2. UV-Visible spectra of the Au₂₅ clusters.

Sedimentation velocity-analytical ultracentrifugation (SV-AUC):

Although the widely accepted chemical protocol was exploited, extreme care has been taken to achieve high quality samples for resonant UPS as to be confident that the main contribution to the UPS signal is from Au₂₅ species. In this regard, SV-AUC experiments were conducted, where the sample size is in the microliter range, analysing the statistical particle ensemble consisting of several tens of millions of clusters, which is orders of magnitude better statistics compared to the standard in which 200 particles are analysed by TEM. Our SV-AUC results show that the sample consists of 88% of Au₂₅ and 12% of aggregates (see Figure S1).

SV-AUC experiments were carried out in an Optima XL-A analytical ultracentrifuge from Beckman Coulter with an absorbance optical detection system and An-60 Ti rotor. Sample solutions (440 mL) were loaded in double-sector Epon centrepieces in a cell with quartz windows. One sector contained Au₂₅ NCs in toluene, with a concentration adjusted so that the absorbance at the monitored wavelength (461 nm) is 0.6 (a.u.). The other sector was filled with pure solvent. The cell/rotor assembly was then placed in the instrument chamber and left under vacuum for at least 6 hrs in order for the temperature to equilibrate.

SV-AUC, a characterization technique orthogonal to TEM and mass spectrometry, was used to determine the purity and the approximate size of Au₂₅ clusters. In this technique, particles in solution are subjected to large gravitational force fields in the centrifuge, leading to sedimentation. The sedimentation process is monitored by a scanning UV/Visible optical detection system that records the absorption profile with respect to radial distance from the rotor (r) and time (t). After measurements are made, a simple hydrodynamic model is applied to convert sedimentation velocity to sedimentation (s) and diffusion (D) coefficients.

SV-AUC experiments were carried at a rotor speed of 42000 rpm at 20 °C. The entire time-course of sedimentation is recorded. Four hundred scans were collected for each cell among which 100 only were kept for further analysis. After noise subtraction and modeling, s and D distributions were generated for Au NCs. This allows us to calculate the molecular weight and relative ratio of gold to ligand.

Figure S2 shows that at least 88% of the sample is comprised of one species with $s = 6.26 \times 10^{-13} \text{ sec}$. The diffusion coefficient corresponding to this species is $D = 3.063 \times 10^{-6} \text{ cm}^2 \text{ s}^{-1}$. The remaining species can be thought of as aggregates of the primary particles. Based on the measured s and D values, we estimate that Au NCs have a molecular weight *ca.* 11.1 kDa, with a density of 2.85 g cm^{-3} , $N_{\text{Au}} \approx 25$ and $N_{\text{SR}} \approx 15$ ligands. These results indicate that the Au NCs have an approximate formula *ca.* Au₂₅(SR)₁₅.

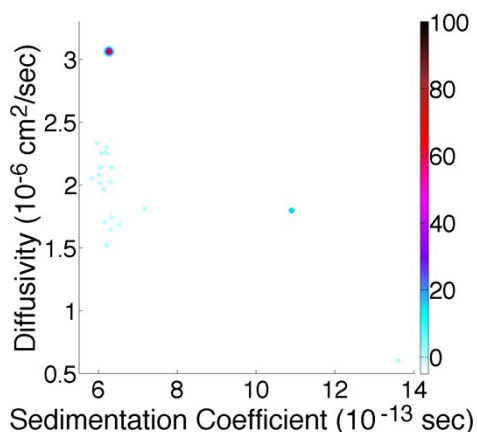


Figure S3. 2D plot of sedimentation coefficients (S) and diffusivities (D) of the species present in the Au sample. Approximately 88% of the sample concentration is at $S = 6.26 \times 10^{-13}$ s and $D = 3.063 \times 10^{-6} \text{cm}^2 \text{s}^{-1}$.

Ultraviolet Photoelectron Spectroscopy (UPS):

The photoemission experiments were performed using the 3m toroidal grating monochromator (3 m TGM) beam line at CAMD in a UHV chamber previously described [1]. The light incident angle of 45° (s+p-polarized light, or with more the vector potential \vec{A} in plane of the surface) in respect to the sample surface normal, making use of the highly linearly polarized light from the synchrotron, as is now commonly done [2, 3]. The filament of electron beam heating system was used to anneal samples up to 100° C by radiation heating. The temperature was measured using K-type of thermocouple attached directly to the sampleplaten. The photoemission spectra were obtained at different photon energies ranging from 65 to 125 eV. Samples were typically prepared by depositing the diluted solution onto a Si(111) sample with a native SiO₂ layer. These spectra taken for 70 to 100 eV range were normalized using photon flux for each energy and after background subtraction the intensities at ~3.5 eV binding energies were plotted versus corresponding binding energies. The combined resolution of the electron energy analyzer and the monochromator was 120 - 150 meV. All binding energies are referenced to the Fermi edge of tantalum foil in electrical contact with the sample. The spectra were normalised to the featureless background level while comparing photoemission intensities.

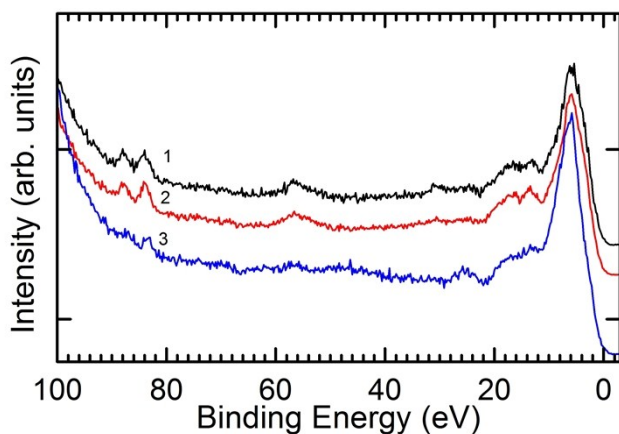


Figure S4. Wide range photoemission spectra of Au mixed-ligand bi-icosahedral structure (Au_{25-bi}) (1, 2) and thiol-stabilized icosahedral core-shell-structure (Au_{25-i}) (3) clusters drop-casted on SiO₂ native oxide surface prepared on Si(111), without sputtering. Photon energy was 125 eV. Note, the annealing at 95° C (2, 3) removes some thiol ligand from Au_{25-i} sample which totally suppresses the Au 4f signal at room temperature for that sample (see Figure 2a). In

contrast, the 4f photoemission of Au is seen even at room temperature (1) for Au_{25-bi} due to desorption of the phosphine ligand under UHV condition.

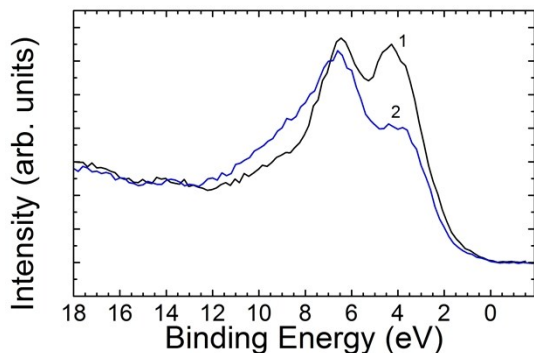


Figure S5. Valence band photoemission spectra of gold mixed-ligand bi-icosahedral structure (Au_{25-bi}) (1) and thiol-stabilized icosahedral core-shell-structure (Au_{25-i}) (2) clusters drop-casted on SiO_2 native oxide surface prepared on Si(111), without sputtering. Photon energy was 70 eV, annealing temperature was 95° C.

The inner-shell 4f electron intensity completely missing in Fig. 2 for the Au_{25-i} sample because of significant screening by thiol ligands. Mild annealing removes some thiols ligands (Figure S4, blue curve 3) and 4f emission become visible.

The shoulder at about of 9 eV binding energy at the spectra in Figure S5, is explained as related to S3p orbitals participated in sulfur-gold bounds. The intensity of this feature correlates with higher sulfur contents in Au_{25-i} in comparison with Au_{25-bi}

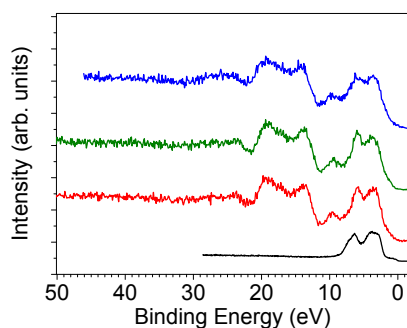


Figure S6. XPS valence band spectra of Au_{25-bi} NC drop-casted onto HOPG (green), quartz (blue) and on SiO_2 native oxide surface prepared on Si(111) (red). The bands in the range from 8 to 18 eV BE are originated from the P 3p, S 3p, C 2s and C 2p states, which are enhanced

by the Al K(alfa) photon energy (compare to valence band on Fig. S5 recorded using 70 eV photons).

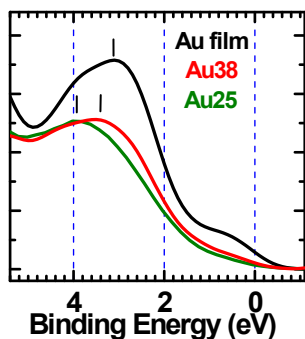


Figure S7. Near Fermi region valence band photoemission spectra of gold mixed-ligand bi-icosahedral structure ($\text{Au}_{25}\text{-bi}$) (green) and thiol-stabilized Au_{38} [4] (red) clusters drop-casted on SiO_2 native oxide surface prepared on $\text{Si}(111)$ and gold film on $\text{Si}(111)$ (black), without sputtering. Photon energy was 80 eV.

All photoemission spectra were scaled to the intensity at the feature-less high energy side of the valence band spectra. The trend of centroid of $5d_{7/2}$ towards higher binding energies is seen as the cluster size decreases.

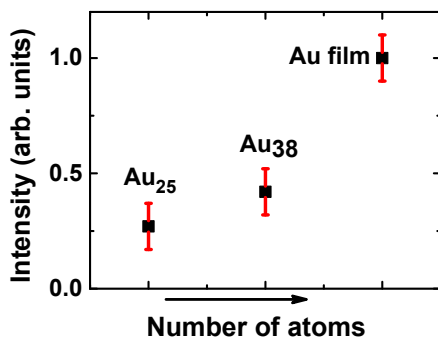


Figure S8. Normalized photoemission intensities in vicinity of Fermi level for Au_{25} , Au_{38} and polycrystalline gold film on $\text{Si}(111)$

Resonant photoemission [5, 14]: The intensity enhancement at a photon energies (85 eV and 87,5 eV) corresponding to the expected shallow $4f_{7/2}$ and $4f_{5/2}$ core level binding energies (83.9 eV and 87.6 eV) relates to the $4f\text{-}5d$ interaction, namely the interaction between a direct photoemission and the direct recombination of an excited state. This means that the normal $5d$

photoemission: $5p^6 4f^{14} 5d^{10-\delta} 6s^1 + h\nu \rightarrow 5p^6 4f^{14} 5d^{9-\delta} 6s^1 + e$ and the decay of the core excitation as $5p^6 4f^{14} 5d^{10-\delta} 6s^1 + h\nu \rightarrow 5p^6 4f^{13} 5d^{11-\delta} 6s^1 \rightarrow 5p^6 4f^{14} 5d^{9-\delta} 6s^1 + e$ interfere. The direct photoemission from the 5d band and photoemission from direct recombination of the hole in the 4f shallow core and a conduction electron in the 5d-6s band (an electron- core hole pair exciton) share the same final states so the photoelectron emitted have the same kinetic energy. The intensity of the 5d spectrum is enhanced. Of course this only works if the $5d^{10}$ is not fully occupied as indicated by $5d^{10-\delta}$. Transitions from 4f to 6s are forbidden without 5d-6s hybridization, and $4f^{14}$ to 5d core exciton formation is forbidden if 5d observes the full d^{10} occupancy. The existence of the photoemission resonance indicates that in fact the full d^{10} occupancy is not observed in these clusters. The fact the resonant intensity is most strong at the $4f_{7/2}$ threshold is consistent with partial occupancy at the top of the 5d envelope, namely for $5d_{5/2}$, not $5d_{3/2}$.

We have performed a series of photon dependent photoemission experiments and plotted an averaged intensity versus photon energy as it is shown in Figure 4. The intensity variation measured at particular photon energy through the number of a series was in the range of indicated error bars. Usually we changed a photon energy with the steps of 0.5-1.0 eV while away from thresholds and with the step of 0.25 eV while passing through threshold. On the plot below we show the data for the $4f_{7/2}$ threshold. Similar, weaker resonance is observed at $4f_{5/2}$ threshold as well. All photoemission spectra were scaled to the intensity at the feature-less high energy side of the valence band spectra. On the Figure S9 we display several selected photoemission spectra otherwise the plot looks confusing and it is hard to see the trend.

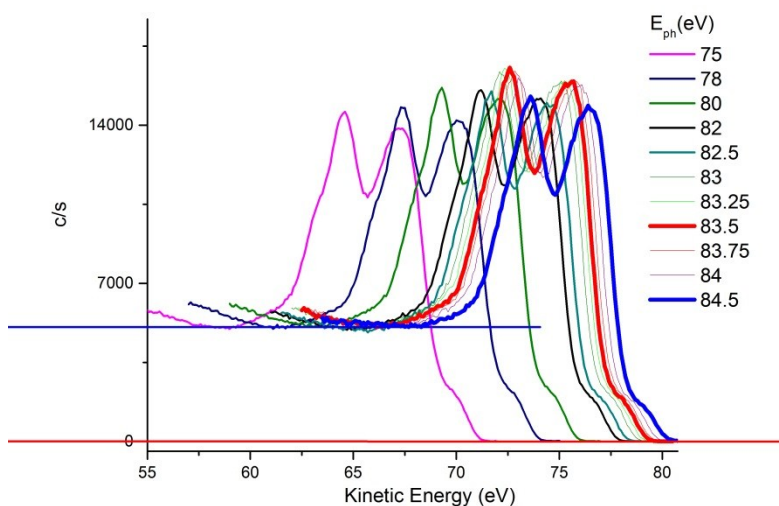


Figure S9. Photoemission spectra of Au₂₅-*bi* clusters drop-casted on SiO₂ native oxide surface prepared on Si(111). Photon energy was tuned across the 4f_{7/2} gold threshold. See text above for details.

We plot both intensities for Au₂₅-*bi* and Au₂₅-*i* in the same graph (Figure 3) with some offset for clarity comparison. The intensity scale for both curves was kept the same, so error bars reflect intensity variation measured at different series. The apparent peak at about 80 eV in the photoemission intensity variations (with photon energy) is the classic behavior of a Fano type resonance. The photoemission intensity slowly increases towards to Cooper minimum [Angle-Resolved Photoemission: Theory and Current Applications; edited by S.D. Kevan, pp 596], by is interrupted by an out-of-phase resonant (anti-resonant) condition below the threshold of the resonant photoemission. Small hump at about of 74 eV could be related to the weak resonance at the 3p threshold, but we can't be here conclusive as the plus and minus error bars overlap for adjacent points for this region.

X-Ray Photoemission Spectroscopy (XPS):

X-ray photoelectron spectra for the Au₂₅ NCs were obtained from samples drop-casted from toluene solution onto a high purity (99.5%) Si substrate. The experiments were performed using a PHI *Versa Probe II* instrument equipped with monochromatic Al K(alpha) source. The X-ray power of 25 W at 15 kV was used for 100 micron beam size at 45° take off angles. The instrument work function was calibrated to give a binding energy (BE) of 84.0 eV for Au 4f_{7/2} line for metallic gold and the spectrometer dispersion was adjusted to give a BE's of 284.8 eV, 932.7 eV and of 368.3 eV for the C 1s line of adventitious (aliphatic) carbon presented on the non-sputtered samples, Cu 2p_{3/2} and Ag 3d_{5/2} photoemission lines respectively. The PHI double charge compensation system was used on all samples. The ultimate Versa Probe II instrumental resolution was determined to be better than 0.125 eV using the Fermi edge of the valence band for metallic silver. XPS spectra in PHI chamber were recorded using software *SmartSoft –XPS* v2.0 and processed using PHI *MultiPack* v9.0 and/or CasaXPS v.2.3.14. Peaks were fitted using GL line shapes a combination of Gaussians and Lorentzians with 30-50% of Lorentzian contents. Shirley background was used for curve-fitting.

Our XPS shows that for Au₂₅-*bi* [Au₂₅(PPh₃)₁₀(SC₁₂H₂₅)₅Cl₂]²⁺ ~80% of phosphine and ~40% of thiol ligands are desorbed in UHV– based on the Au/P and Au/S ratio. In case of Au₂₅-*i* [Au₂₅(SCH₂CH₂Ph)₁₈]- – it maintains its stoichiometry, i.e. Au/S=25/18.

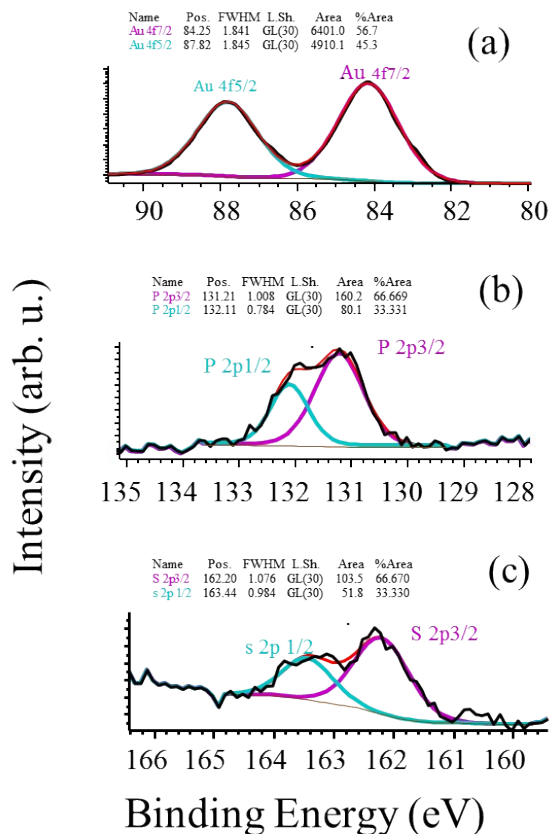


Figure S10. XPS spectra of (a) Au 4f, (b) P 2p, and (c) S 2p Au₂₅-*bi* NC. The Au/S ratio is 1 and Au/P ratio is 10 i.e. desorption of ~ 50% thiol ligands and ~ 80% phosphine ligands takes place (overall, 11 out of 15 ligands have desorbed). Monochromatic Al K(alpha) source ($E_{ph}=1486.6$ eV) was used for all spectra.

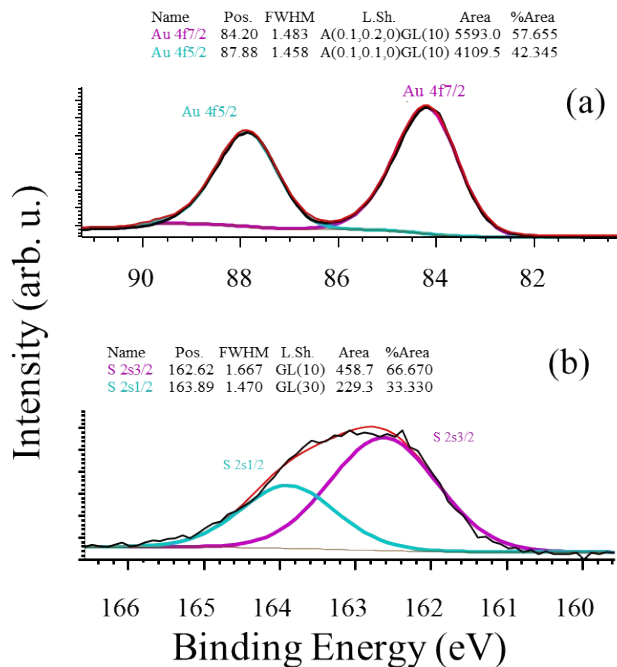


Figure S11. XPS spectra of (a) Au 4f and (b) S 2p Au_{25-i} NC. Au/S peak ratio is 1.4, i.e. the stoichiometric composition is preserved (the nominal ratio is 1.39).

The asymmetric line shape was used in order to obtain better fit results for Au_{25-i}. Monochromatic Al K(alpha) source ($E_{ph}=1486.6$ eV) was used for all spectra.

Grazing Incident Wide-Angle X-ray Scattering (GIWAXS):

GIWAXS experiments were performed on D-line, Cornell High Energy Synchrotron Source (CHESS) at Cornell University. The X-ray with a wavelength of 1.15Å in a wide band pass (1.47%) shinned on the sample at the incident angle of 0.15°. A Pilatus 100K detector was placed 225 mm away from the sample to collect the scattering signal in the exposure time of 1s. A 1.5 mm-wide tantalum rod was used to block the intense scattering in the vicinity of the direct beam. The inter-particle spacing is 1.91nm from the (001) peak in GIWAXS pattern.

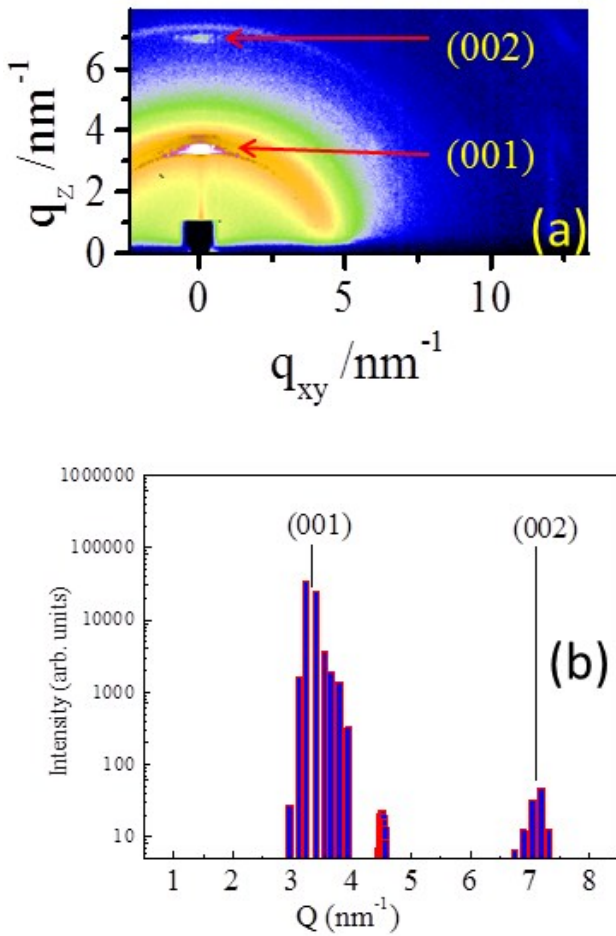


Figure S12. (a) GIWAXS plot. (b) Profile along q_z axis at $q_{xy}=0$.

Calculation details:

The calculations were implemented in VASP code [6, 7] with projector augmented-wave (PAW) method [8,9], plane wave basis set with cutoff energy of 400 eV, and generalized gradient approximation (GGA) within the parameterization of Perdew-Burke-Ernzerhof (PBE) [10]. Monkhorst-Pack [11] $3 \times 3 \times 1$ k-point grid was adopted for the Brillouin zone sampling. The coordinates of the atoms are optimized until the max force on each atom is smaller than 0.02 eV/Å.

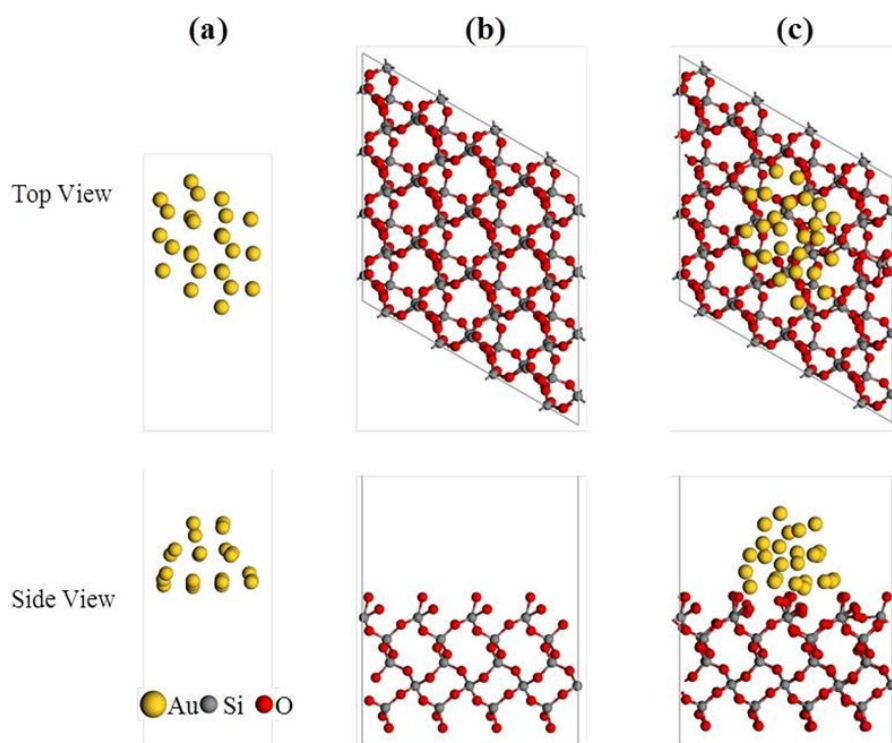


Figure S13. Optimized structures of (a) Au₂₅ cluster, (b) SiO₂(111) surface slab, and (c) Au₂₅ cluster adsorbed on SiO₂(111) surface slab.

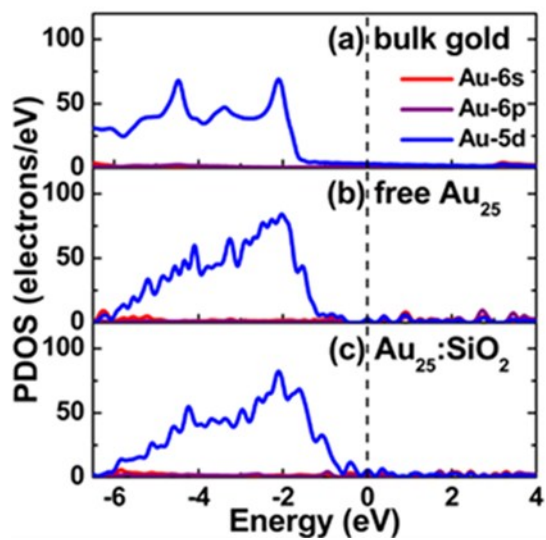


Figure S14. Density of states for (a) bulk Au, (b) the gas phase free Au₂₅ cluster, and (c) Au₂₅ adsorbed on SiO₂(111) surface. Black dash lines indicate the Fermi levels.

Chemicals and Solvents:

Tetrachloroauric (III) acid ($\text{HAuCl}_4 \cdot 3\text{H}_2\text{O}$, >99.9% metals basis, Aldrich), Triphenylphosphine (>98.5%, Aldrich), 1-Dodecanethiol (>98%, Aldrich), Tetraoctylammonium bromide (TOAB, 98%, Aldrich), 2-phenylethanethiol ($\text{PhCH}_2\text{CH}_2\text{SH}$, 99%, Aldrich), Sodium borohydride (>98%, Aldrich). tert-Butyl hydroperoxide solution (TBHP, ~5.5 M in decane, Aldrich). Tetrahydrofuran (THF, HPLC grade, $\geq 99.9\%$), Acetonitrile (>99.9%, Aldrich), Ethanol (Aldrich), 2-propanol (HPLC grade), Toluene (HPLC grade, $\geq 99.9\%$), Methylene chloride (HPLC grade, $\geq 99.9\%$). All chemicals were used without any purification. Nanopure water is used in all experiments.

Synthesis procedure for $\text{Au}_{25}\text{-bi}$ clusters:

$[\text{Au}_{25}(\text{PPh}_3)_{10}(\text{SC}_{12}\text{H}_{25})_5\text{Cl}_2]^{2+}$ clusters possessing both phosphine and thiol ligands were prepared using a modified literature procedure [12]. In a typical synthesis, 500 mg (1.5 mmol) of $\text{HAuCl}_4 \cdot 3\text{H}_2\text{O}$ was dissolved in 100 mL of THF. 3 mmol of PPh_3 was added to this stirring solution followed by drop wise addition of 30 mL of ethanolic 0.15 M NaBH_4 solution over 30 min for reduction. 4.5 mmol of 1-dodecanethiol was added to this reaction mixture and the solution was allowed to stir for 24 h at room temperature. The solution was washed once with water, and the solvent from the organic fraction was evaporated under nitrogen flow. The solid material was then dissolved in 200 mL of n-pentane and transferred to a separatory funnel. The solution was extracted with 100 mL portions of acetonitrile until the acetonitrile layer was colorless. The acetonitrile was removed under nitrogen flow, and the solid was dissolved in a minimum amount of 2-propanol. The crude product was then loaded on a silica gel column (mobile phase 3:1 2-propanol/toluene). The late eluting brown band was collected, and the solvent was removed under vacuum.

Synthesis procedure for $\text{Au}_{25}\text{-i}$ clusters:

Thiol-stabilized $[\text{Au}_{25}(\text{SCH}_2\text{CH}_2\text{Ph})_{18}]^-$ clusters were prepared using a reported procedure [13]. Briefly, 0.4 mmol (0.157 g) of $\text{HAuCl}_4 \cdot 3\text{H}_2\text{O}$ was dissolved in 5 mL of Nanopure water and mixed with a solution containing 0.47 mmol (0.255 g) of TOAB in 10 mL of toluene taken in a 50 mL round bottom flask. The mixture was stirred vigorously for ~10 min using magnetic stir bar to transfer the Au(III) salt into the organic phase. The aqueous layer was then removed using a syringe. The toluene solution containing the gold salt was purged with N_2 and then cooled to 0

°C using an ice bath over a period of 30 min under magnetic stirring. The solution was kept at the same temperature and 0.17 mL of PhCH₂CH₂SH (2-phenylethanethiol) was added and the stirring was reduced to very low speed. The deep red solution turned to faint yellow in 5 min and became colorless over 1 h. Once the solution turned to clear (~1 h), the stirring speed was increased to fast stirring. Maintaining the same temperature (*i.e.* 0 °C), immediately an aqueous solution of NaBH₄ (0.1550g, 4 mmol) freshly prepared in 7 ml ice-cold nanopure water was quickly added. The reaction was allowed to proceed overnight under N₂ atmosphere. After overnight, the ice bath is removed and the aqueous layer at the bottom of the flask was removed using a syringe, and the toluene solution was dried. Ethanol (~20 mL) was added to separate Au_{25-*i*} clusters from TOAB and side products. The Au_{25-*i*} clusters were collected after removing the supernatant and purified by extracting twice with acetonitrile.

Mass Spectrometry: MALDI mass spectra were acquired from Bruker Omnix mass spectrometer using DCTB matrix at optimal laser fluence. ESI mass spectra were obtained from Waters Synapt mass spectrometer in positive mode.

Matrix-Assisted Laser Desorption Ionization – Time of Flight (MALDI-TOF) spectra of the Au₂₅-i clusters:

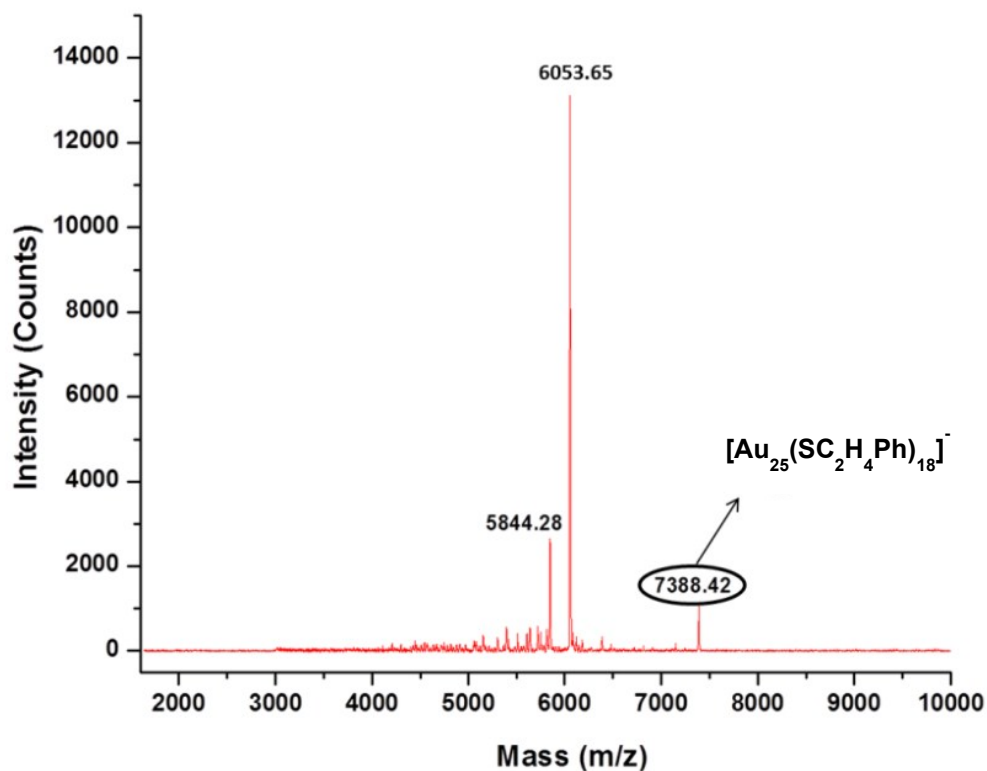


Figure S15. . MALDI-TOF spectra of Au₂₅-i clusters

Electrospray Ionization (ESI) spectra of Au₂₅-bi clusters:

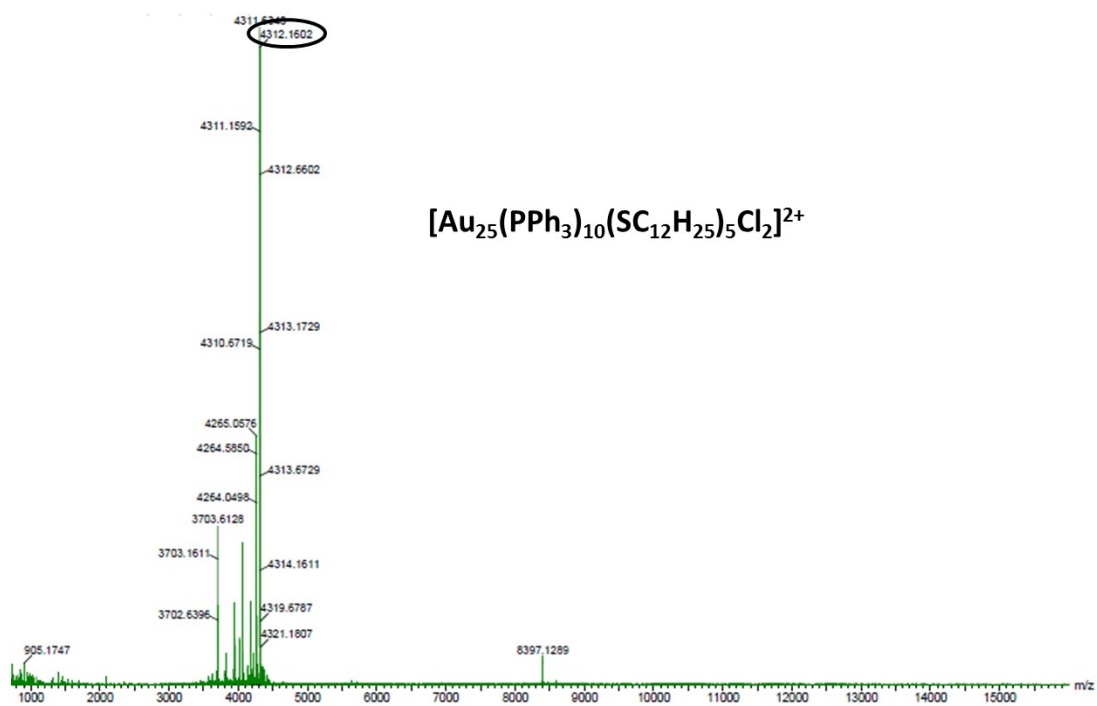


Figure S16. ESI spectra of Au₂₅-bi clusters.

References:

- [1] Dowben, P. A.; LaGraffe, D.; Onellion, M. *J. Phys. Cond. Matt.* **1989**, *1*, 6571.
- [2] Eberhardt, W.; Plummer, E.W. *Phys. Rev. B* **1980**, *21*, 3245.
- [3] Losovyj, Y.; Ketsman, I.; Wang, Z.; Tang, J.; Dowben, P. *Nucl. Instrumen. Meth. A* **2007**, *582*, 264.
- [4] Y. B. Losovyj, S.-C. Li, N. Lozova, K. Katsiev, D. Stellwagen, U. Diebold, L. Kong and C. S. S. R. Kumar, *J. Phys. Chem. C*, 2012, *116*, 5857-5861.
- [5] Lapeyre, G. J., Anderson, J., Gobby, P. L., and Knapp, J. A., *Phys. Rev. Lett.* **1974**, *33*, 1290
- [6] Kresse, G.; Furthmuller, J. *Phys. Rev. B* **1996**, *54*, 11169.
- [7] Kresse, G.; Furthmuller, J. *Comput. Mater. Sci.* **1996**, *6*, 15.
- [8] Blochl, P. E. *Phys. Rev. B* **1994**, *50*, 17953.
- [9] Kresse, G.; Joubert, D. *Phys. Rev. B* **1999**, *59*, 1758.
- [10] Perdew, J. P.; Burke, K.; Ernzerhof, M. *Phys. Rev. Lett.* **1996**, *77*, 3865.
- [11] Monkhorst, H. J.; Pack, J. D. *Phys. Rev. B* **1976**, *13*, 5188.
- [12] Shichibu, Y.; Negishi, Y.; Watanabe, T.; Chaki, N. K.; Kawaguchi, H.; Tsukuda, T. *J. Phys. Chem. C* **2007**, *111*, 7845.
- [13] Zhu, M.; Lanni, E.; Garg, N.; Bier, M. E.; Jin, R. *J. Am. Chem. Soc.* **2008**, *130*, 1138.
- [14] P. A. Brühwiler, A. J. Maxwell, A. Nilsson, R. L. Whetten and N. Mårtensson, *Chemical Physics Letters*, 1992, *193*, 311-316.